water

Article

Experimental and Theoretical Explanations for the Initial Difference in the Hydraulic Head in Aquitards

Yongliang Xu [1], Chaoyang Du [2,*], Haizhi Ma [1], Wei Pang [1], Suhang Huang [1] and Shimin Li [1]

[1] Beijing Key Laboratory of Geotechnical Engineering for Deep Foundation Pit of Urban Rail Transit, Beijing Urban Construction Exploration & Surveying Design Research Institute Co., Ltd., Beijing 100101, China
[2] Key Laboratory of Water Cycle and Related Land Surface Processes, Institute of Geographic Sciences and Natural Resources Research, Chinese Academy of Sciences, Beijing 100101, China
* Correspondence: ducy@igsnrr.ac.cn

Abstract: Accurate estimation of the buoyancy forces exerted on underground structures is a problem in geotechnical engineering that directly impacts the construction safety and cost of these structures. Therefore, studying the buoyancy resistance of underground structures has great scientific and practical value. In this study, an initial difference in the hydraulic head, Δh_0, was discovered to be present in aquitards through analysis of water-level data collected from the observation of real-world structures and in laboratory control tests. That is, seepage occurs beyond a threshold Δh_0. Analysis of test data reveals that a deviation from Darcy's law is the theoretical basis for Δh_0 and that Δh_0 equals the initial hydraulic gradient multiplied by the length of the seepage path. The general consistency between the experimentally measured and theoretically calculated values of Δh_0 validates the theoretical explanation for Δh_0. The results of this study provide a basis for scientifically calculating the buoyancy resistance required for the construction of underground structures.

Keywords: model test; groundwater buoyancy; initial head difference; initial hydraulic gradient; aquitard

check for updates

Citation: Xu, Y.; Du, C.; Ma, H.; Pang, W.; Huang, S.; Li, S. Experimental and Theoretical Explanations for the Initial Difference in the Hydraulic Head in Aquitards. *Water* **2022**, *14*, 3042. https://doi.org/10.3390/w14193042

Academic Editor: Yu Huang

Received: 27 July 2022
Accepted: 21 September 2022
Published: 27 September 2022

Publisher's Note: MDPI stays neutral with regard to jurisdictional claims in published maps and institutional affiliations.

Copyright: © 2022 by the authors. Licensee MDPI, Basel, Switzerland. This article is an open access article distributed under the terms and conditions of the Creative Commons Attribution (CC BY) license (https://creativecommons.org/licenses/by/4.0/).

1. Introduction

Urban development has led to the construction of large numbers of underground structures that, together with groundwater and soil masses, form complex systems in which these structures interact. Due to the presence of groundwater, these systems can cause a multitude of problems to real-world underground structures. Buoyancy resistance is prominent among these problems [1]. Apart from being a major problem in geotechnical engineering, buoyancy resistance is also a challenging issue encountered with real-world underground structures that directly impacts their safety and cost. Therefore, studying the buoyancy resistance of underground structures has great scientific and practical value [2,3].

In current engineering practice, groundwater in formation layers is generally regarded as static water, and the buoyancy forces on underground structures from groundwater are calculated using Archimedes' principle. The interparticle pores in sand and pebble layers are large. As a result, free water that fills these pores is able to move freely between the particles. Therefore, Archimedes' principle is suitable for highly permeable beds [4,5]. Extensive experimental results show that this approach is applicable to such highly permeable layers composed of sand and pebbles [6,7].

Aquitards composed of clayey soil have low connectivity due to the presence of particle-bound water. Therefore, calculating the buoyancy forces on underground structures in aquitards is a complex task. Relevant research results differ considerably [8–11]. Some studies have shown a high level of consistency between the buoyancy forces measured in experiments and those calculated using Archimedes' principle [12–15]. Cui et al. (1999) determined the buoyancy force on an underground structure in two media (sandy and clayey soils) in a model test and did not find a significant reduction in the pore-water pressure (PWP) [16]. Through extensive laboratory tests, Zhang and Chen (2008) found that the PWP reduction coefficient of bound water in clayey soils is very small, so as to be negligible in real-world engineering scenarios [12]. Xiang et al. (2010) experimentally demonstrated that saturated clayey soils in a long-term stable state can fully transfer PWP and that the effects of bound water do not need to be considered [17]. In contrast, other studies have reported an appreciable difference between the buoyancy forces measured in experiments and those calculated using Archimedes' principle, while noting that a reduction in the theoretical value needs to be considered in the calculation of the buoyancy force from groundwater in clayey soils and introducing methods to determine the reduction coefficient [18–20]. Zhou et al. (2019) experimentally determined the variation in the buoyancy force on an underground structure in an aquitard with depth and found that the reduction coefficient increased from 0.25 to 0.52 as the depth increased [3]. Song et al. (2017) conducted an experiment in which the half-interval search method was used to determine the buoyancy forces exerted by groundwater on foundations embedded in clay soil [19]. They found that the measured buoyancy forces on foundations in clay soil were lower than the corresponding theoretical values but were consistent with large-scale field measurements. Zhang et al. (2019) experimentally evaluated the buoyancy effect on underground grain silos in sandy and clayey soils and determined the values (0.95 and 0.79, respectively) of the buoyancy reduction coefficient for these two types of soils [21]. Zhang et al. (2018) analyzed the patterns of variation in the PWP with depth in sandy and clayey soils through centrifugal model tests and found the following. (1) The measured values of the PWP were consistent with its theoretical values in sandy soils, while the measured values of the PWP were lower than its theoretical values in clayey soils. (2) The PWP reduction coefficient varied with depth and stabilized at approximately 0.68 at depths greater than 10 m [22]. By designing and conducting model tests at multiple scales, Zhou (2006) found that groundwater buoyancy in clay layers is only 75% of the conventional theoretical value [18]. Despite the substantial experimental efforts in the abovementioned studies, a consensus has yet to be established on the reduction in water buoyancy in clay layers. Research on the theoretical basis of the reduction phenomenon lacks depth.

Currently, the reduction coefficient (i.e., the ratio of the measured value to the theoretical value) is still used to depict the reduction in water buoyancy in clay layers. This method neglects the lack of a direct proportional relationship between the measured and theoretical values of buoyancy. The line of best fit between the experimentally measured and theoretical values of groundwater buoyancy in clay layers has an intercept that is defined in this study as the "initial difference in the hydraulic head h, Δh_0." This study attempts to demonstrate the presence of Δh_0 in aquitards through model-based continuous buoyancy monitoring tests and provide a theoretical explanation for Δh_0, which is subsequently validated based on measurements.

2. Materials and Methods

2.1. Tests

It is exceedingly difficult to measure the buoyancy force on a real-world underground structure and impossible to artificially control its boundary conditions in the field. In comparison, the boundary conditions (e.g., the surrounding soil layer, water level H, and lateral resistance) of an underground structure module (USM) can be controlled in a laboratory test setting. Hence, laboratory tests were conducted in this study to experimentally and theoretically explain the Δh_0 in aquitards.

(1) Test design

External environmental elements (i.e., a soil layer and groundwater) are required to determine the variation in the buoyancy force on a USM in a silty soil layer with known water-supply conditions. To achieve this, a model test box (MTB) consisting of a USM, an enclosure structure module (ESM), a test soil layer, a water-supply system, and monitoring systems was employed to conduct continuous buoyancy monitoring tests. The design of the MTB allowed the test soil layer to be replaced, the delivery head h_d to be adjusted, and the H in the test soil layer (H_s) and the buoyancy force exerted by the water on the USM (F_2) to be monitored in real time.

The USM consisted of a rigid circular steel plate and a tetrahedron. The rigid circular steel plate was located on the bottom of the ESM and overlain by the tetrahedron, which served as a fulcrum for a tension–compression sensor located above the USM.

The ESM, composed of a rigid cylinder and a waterproof rubber bottom, ensured that the enclosure structure was devoid of water during the test. Moreover, the internal USM was not placed in direct contact with the wall of the enclosure to prevent lateral friction.

Silty clay and fine sand were employed as the two types of soil layers in the test. The silty clay layer, representing aquitards, was the focus of this study. The fine sand layer, representing highly permeable layers, was used to examine the reliability of the test model. The F_2 monitoring test results obtained using the two layers were compared.

The water-supply system consisted of an external water tank, an inlet pipe, and an inverted filter layer. The external water tank was used to adjust h_d. The inlet pipe, made of a plastic flexible tube, connected the external water tank and MTB. The inverted filter layer, composed of medium sand, was primarily used to ensure a uniform water supply to the test soil layer above it.

The MTB was equipped with three systems to monitor h_d, H_s, and F_2, respectively. A PWP sensor was used to automatically monitor h_d. Similarly, PWP sensors were also used to automatically monitor the H_s at seven observation holes located at different depths. A tension–compression sensor was employed to automatically monitor F_2.

(2) Composition of the test setup

The test setup consisted mainly of an MTB, a test soil layer, a tetrahedron, a rigid circular steel plate, an enclosure structure, waterproof rubber, a reaction beam, H_s observation holes, a water-supply tank, and an inverted filter layer. Figures 1 and 2 show the test setup in detail.

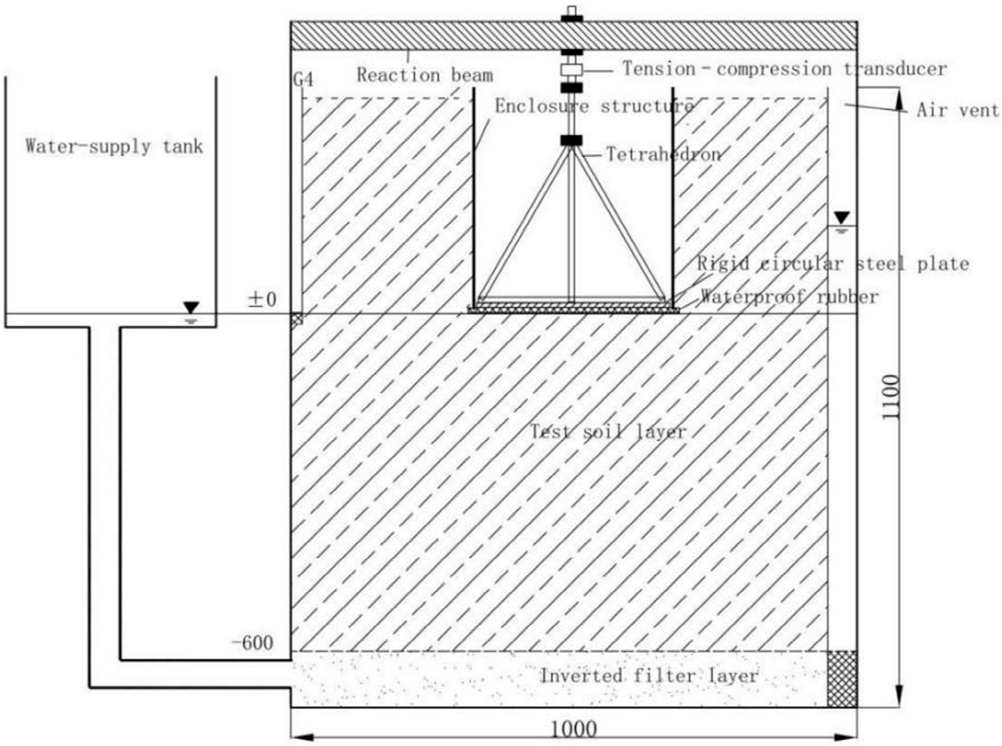

Figure 1. Cross-sectional schematic of the MTB (units: mm).

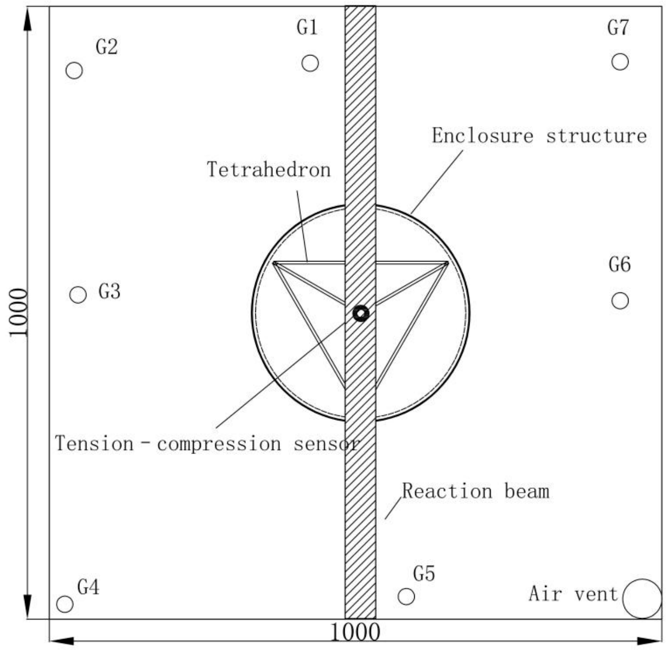

Figure 2. Top view of the MTB (units: mm).

The MTB was 1000 mm long, 1000 mm wide, and 1100 mm tall. The enclosure structure consisted of a bottomless steel cylinder with a height of 400 mm and an inner diameter of 350 mm. The USM was composed of a tetrahedron and a rigid circular steel plate with an outer diameter of 335 mm. Throughout the test, water was supplied laterally to the bottom of the MTB. Seven H_s observation holes were prepared in the test soil layer at depths of 200, 300, 400, 500, 600, 700, and 800 mm. These holes are denoted by G1, G2, G3, G4, G5, G6, and G7, respectively. A 2 cm-long filter was placed at the bottom of each hole to observe the H_s at the corresponding depth. A 10 cm-thick inverted filter layer composed of medium sand was placed at the bottom of the MTB and was overlain by the test soil layer. The micro-PWP and tension–compression sensors used in the MTB were custom-made products (Figures 3 and 4). Table 1 summarizes their basic parameters.

Figure 3. Micro-PWP.

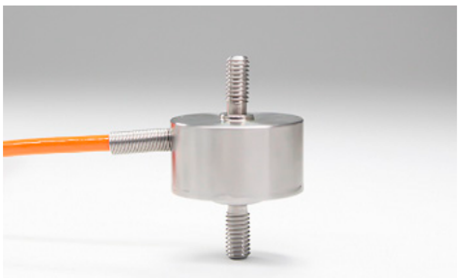

Figure 4. Tension–compression sensor.

Table 1. Sensor parameters.

Name	Type	Measuring Range	Composite Error (%F·S)	Diameter × Thickness (mm)	Material	Impedance (Ω)
Micro-PWP sensor	YSV3201	0–30 kPa	≤0.05	Φ15 × 20	Stainless steel	350
Tension–compression sensor	H-2	0–100 kg	≤0.05	Φ40 × 30	Stainless steel	400 ± 10

(3) Test procedure

The test procedure is detailed in Figure 5 below.

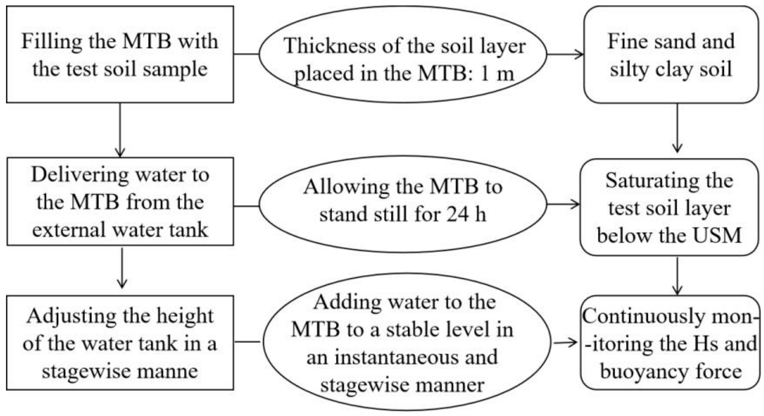

Figure 5. Flowchart of the test procedure.

(1) Soil-sample preparation and filling. The fine sand and silty clay used in the tests were both retrieved from construction sites in Changchun. In this study, the effects of structured soils on test results were not considered. Therefore, remolded soils were used instead of undisturbed soils. The retrieved soil samples were manually crushed in the laboratory. Each soil sample was sprayed sparingly with water while being placed in the MTB layer by layer. Each layer was no thicker than 20 cm and was manually compacted before the subsequent layer was placed on top of it. The same procedure was followed to fill the MTB with each of the two test soil samples (i.e., fine sand and silty clay). Tables 2 and 3 summarize the physical property metrics of the test soil samples placed in the MTB. The fine sand layer was first tested to examine test reliability. Subsequently, a continuous F_2 monitoring test was performed with the silty clay layer;

Table 2. Physical property metrics of the fine sand sample used in the test.

Test Soil Sample	Moisture Content W/%	Wet Density ρ/(g·cm^{-3})	Porosity e	Saturation Sr/%	Dry Density ρd/(g·cm^{-3})	Permeability Coefficient k (cm·s^{-1})
Sand	26.7	1.96	0.64	96.1	1.63	5.59×10^{-3}

Table 3. Physical property metrics of the silty clay sample used in the test.

Test Soil Sample	W/%	ρ/(g·cm^{-3})	Porosity n/%	Sr/%	ρd/(g·cm^{-3})	Plasticity Index Ip	Liquidity Index IL	Permeability Coefficient k (cm·s^{-1})
Silty clay	21.1	1.71	44.6	95.9	1.35	13.4	0.46	1.45×10^{-5}

(2) Delivery of water from the external water tank. The external water tank was used to provide a continuous water supply to the MTB. h_d was kept at the same level as the

bottom of the rigid circular steel plate in the MTB. The H_s in the MTB was monitored continuously. After H_s stabilized, the MTB was allowed to stand still for 24 h to allow the test soil layer beneath the USM to be completely saturated;

(3) F_2 monitoring test. The height of the water-supply tank was adjusted to increase h_d in a stagewise manner. The extent to which h_d was increased at each stage depended on the H_s and F_2 response speed inside the MTB. At the start of each stage, water was added to the water tank to maintain a stable h_d for a certain period of time, after which the addition of water was terminated. After H_s stabilized, h_d was increased again to commence the subsequent stage of the test. Throughout the test, H_s and F_2 were monitored automatically and in real time.

To facilitate subsequent discussion and analysis, the bottom of the rigid circular steel plate was used as a reference surface (i.e., the initial h) in each test.

2.2. Force Analysis

Because the USM was not subject to lateral friction in the test, only the vertical forces are analyzed. Figure 6 shows the forces acting on the USM, as determined according to the principle of static equilibrium. The equilibrium equation is given below.

$$F_1 + F_2 = G_0 + P_\mathrm{s} \tag{1}$$

where G_0 is the dead weight of the USM (N), P_s is the pressure detected by the tension–compression sensor (N), F_1 is the vertical reaction from the soil particles (N), and F_2 is the buoyancy force exerted by the groundwater (N).

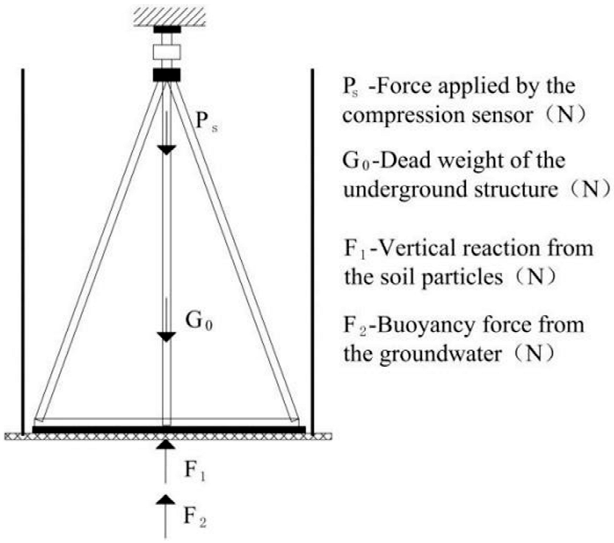

Figure 6. Force analysis of the USM.

Water was initially delivered into the MTB to allow H_s to be flush with the bottom plate of the USM. Under this condition, F_2 = 0 and P_s was a fixed value (P_{s0}; 338 and 250 N in the fine sand and silty clay layers, respectively). Based on Equation (1), $F_1 = P_{s0} + G_0$ (G_0 = 39.9 N). The test was started by increasing H_s. The variation in the reading of the tension–compression sensor was in fact the variation in the total pressure of the water and soil due to the comprehensive action of F_2. Therefore, F_1 is assumed to have remained constant throughout the test, while the variation in the total pressure is regarded as F_2. The following equation holds in a stable state:

$$F_2 = P_\mathrm{s} - P_0 \tag{2}$$

The measured F_2 (mm) is converted to h (h_b, the buoyancy head), i.e.,

$$h_b = F_2/Ag \tag{3}$$

where A is the area of the bottom of the rigid circular steel plate with a diameter of 335 mm (88,141.31 mm^2) and g is the gravitational acceleration (10 N/kg).

Considering that limited test data were obtained, the measured data were fitted to reflect the variation trend in h_b for all h_d values.

3. Results and Discussion

3.1. Presence of Δh_0

3.1.1. Presence of Δh_0 in the Tests

The values of F_2 in the fine sand and silty clay layers were monitored. The dynamic variation in F_2 under instantaneous water-supply conditions was determined. The relationship between the stable h_d and F_2 was analyzed through comparison.

(1) Dynamic variation in F_2 under instantaneous water-supply conditions.

Figures 7 and 8 show the patterns of dynamic variation in F_2 in the fine sand and silty clay layers, respectively, as determined based on the values of h_d and h_b obtained from the tests.

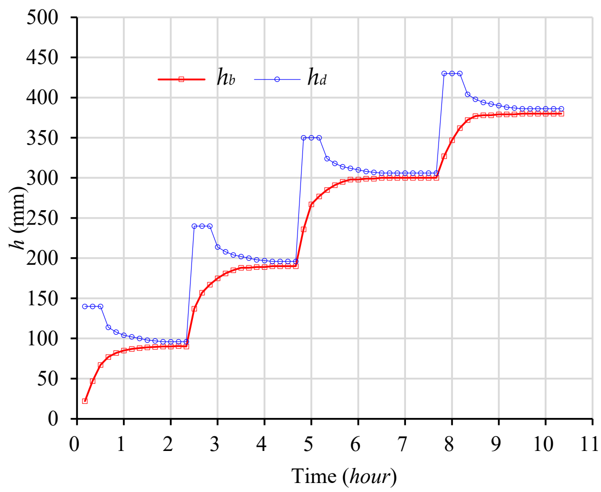

Figure 7. Variation in h_d and h_b during the test conducted in fine sand.

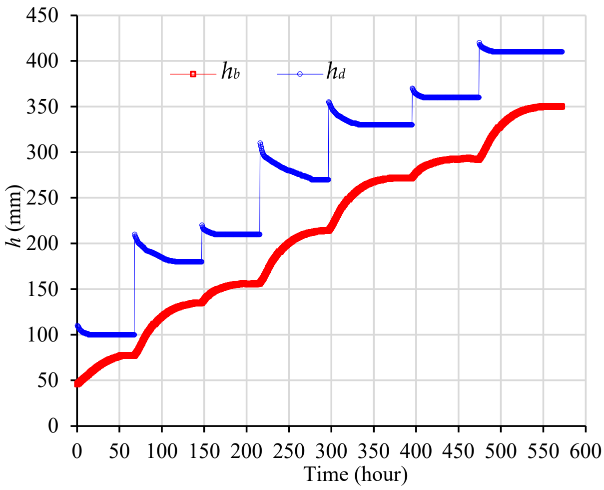

Figure 8. Variation in h_d and h_b during the test conducted in the silty clay layer.

Figures 7 and 8 show that after h_d was increased instantaneously at each stage, the H in the water-supply tank decreased with time, while F_2 gradually increased. The F_2 acting on the USM in the fine sand layer responded rapidly to h_d. The test conducted in the fine sand layer involved four stages and lasted for 10.5 h in total. During the first 0.5 h of each stage, water was continuously delivered into the MTB, resulting in a rapid increase in h_b. Two hours later, h_b tended to stabilize. The measured value of h_b in the fine sand layer was almost the same as the value of h_d. The F_2 acting on the USM in the silty clay layer responded slowly to h_d. The test conducted in the silty clay layer involved seven stages and lasted for approximately 572 h in total. On average, it took 60 h for h_b to stabilize during each stage. The stable value of h_b was appreciably lower than the value of h_d.

A comparison of Figures 7 and 8 shows the following. The measured value of F_2 acting on the USM in the simulated highly permeably layer was basically consistent with its theoretical value, suggesting no reduction in h. In contrast, the measured value of F_2 acting on the USM in the simulated aquitard was considerably lower than its theoretical value, suggesting a reduction in h.

(2) Comparison of the stable h_d and h_b.

After water was instantaneously delivered into the MTB during each stage, h_d and h_b eventually became stable and remained unchanged. Under this condition, the groundwater throughout the MTB was in a static state. The stable values of h_d and h_b were linearly fitted for analysis, as shown in Figure 9a,b.

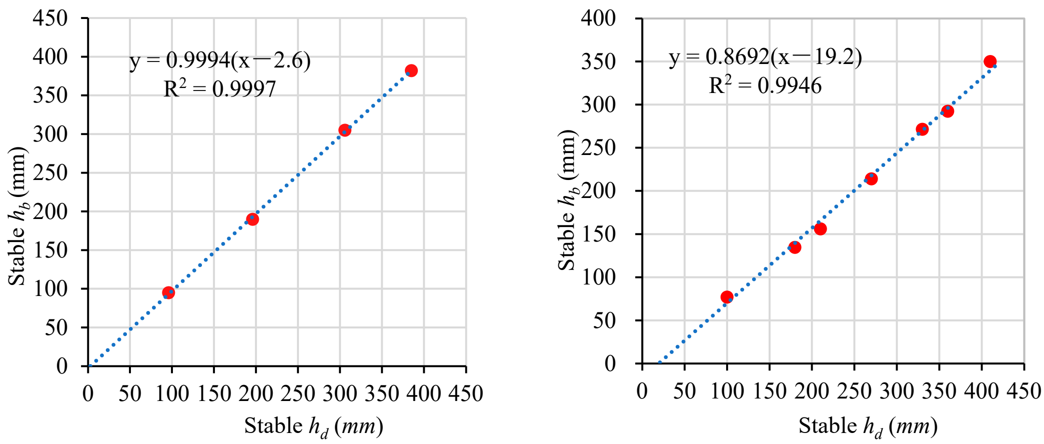

(**a**) Fine sand layer (**b**) Silty clay layer

Figure 9. Relationship between the stable h_d and h_b during a test conducted in the fine sand and silty clay layers.

Figure 9a shows a slope of nearly 1 for the line of best fit between the stable h_d and h_b measured during the test conducted in the fine sand layer, suggesting no reduction in h in the simulated highly permeable layer. The transverse intercept of the line of best fit shown in Figure 9a is 2.6 mm, which can be ascribed to experimental error and is negligible.

In Figure 9b, the stable h_d is not directly proportional to the stable h_b determined during the test conducted in the silty clay layer. The line of best fit between the stable h_d and h_b does not pass through the origin. A transverse intercept of 19.2 mm can be observed for H_s at the bottom of the USM. Analysis of the linear fitting equation reveals that there is no h_b for the USM when h_d is smaller than this transverse intercept and that F_2 only occurs when h_d exceeds this transverse intercept. This transverse intercept is defined in this study as the initial difference in h, Δh_0. Observation of the lines of best fit shows a prominent Δh_0 in the silty clay layer that plays a significant role in the calculation of F_2.

3.1.2. Presence of Δh_0 in Real-World Engineering Settings

Δh_0 can also be found during routine drilling operations. A confined aquifer is overlain by a thick silty clay layer. A dry soil or unsaturated wet soil layer is encountered during the initial stage of drilling in the silty clay layer. This layer is referred to as the vadose zone. Further drilling in the silty clay layer exposes free water. An H that remains unchanged for a prescribed period of time after the drilling operation is paused is often taken as the stable initial H (H_0) (Figure 10a). A saturated zone is encountered as the drilling depth increases. Here, the stable H observed in the borehole continues to increase (Figure 10b,c). The stable H in the borehole is exactly the same as the confined H (H_c) in the aquifer when the borehole just reaches the confined aquifer (Figure 10d). At this location, the H_c is significantly higher than the stable H_0.

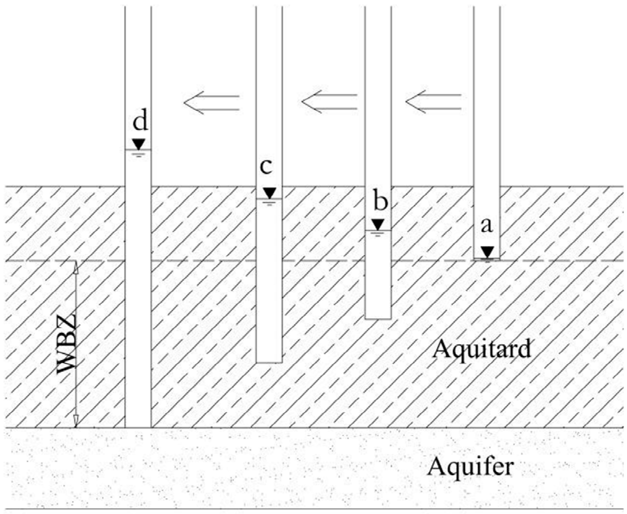

Figure 10. Schematic showing the variation in H observed during drilling of a confined aquifer [23] ((**a**): Stable initial water table; (**b**,**c**): Stable water table observed at different depths after entering the unsaturated zone; (**d**): Stable water table in confined aquifer).

Zhang (1980) referred to the saturated layer between the location of the stable H_0 and the roof of an aquifer as the water-bearing zone (WBZ) of the aquitard above the aquifer [23]. An underground structure in a WBZ is subject to a positive buoyancy force from water. However, because the H in a WBZ is invariably lower than the H_c, the measured value of the buoyancy force from the water in the WBZ is invariably lower than the value calculated based on the H_c. The Δh_0 at a specific location in a WBZ equals the H_c minus the H at the location. The Δh_0 in a WBZ equals the h of the confined water minus the stable H_0. When the H_c remains stable and unchanged, the stable H_0 also remains unchanged. As the H_c increases, the difference in h (Δh) surpasses the Δh_0 in the original stable state. As a result, groundwater begins to seep upward in the silty clay layer, accompanied by an increase in the stable H_0.

3.2. Theoretical Explanation for Δh_0

Under normal circumstances, the seepage velocity V of groundwater in a formation layer is directly proportional to the hydraulic gradient I according to the well-known Darcy's law. However, some researchers obtained results from laboratory seepage tests conducted in saturated silty clay layers that deviate from Darcy's law [20,24–26]. These test results show that the V–I curve for a clay layer does not pass through the origin, that no seepage occurs when I is lower than a certain value I_0, and that the V–I curve is a straight line when $I > I_0$ (Figure 11).

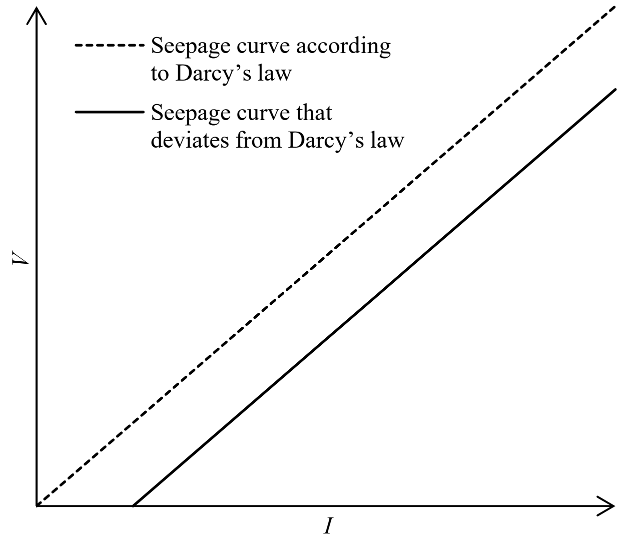

Figure 11. V–I curves from seepage tests.

The seepage curve deviates from Darcy's law, as shown in Figure 11, and can be described using the approximate expression proposed by Poza (1950) shown below [27]:

$$V = K\,(I - I_0) \tag{4}$$

the intercept I_0 of the above equation is the initial I often mentioned in the context of groundwater seepage flow.

In the critical seepage state when $I = I_0$, I_0 equals the ratio of the Δh in the critical seepage state (i.e., Δh_0) to the length of the corresponding seepage path, L_0, as expressed below.

$$I_0 = \Delta h_0 / L_0 \tag{5}$$

The Δh in the critical seepage state is the initial Δh (i.e., Δh_0). In other words, Δh_0 exists in a test soil layer with a certain thickness. When the Δh between the two sides of the seepage path is smaller than Δh_0, the groundwater is in a static state. The groundwater is only able to seep through the soil layer when the Δh between the two sides of the seepage path is greater than Δh_0. Therefore, in the tests conducted in this study, when $h_d < \Delta h_0$, the groundwater did not seep through the test soil layer and rise above the bottom of the USM. As a result, the USM was not subject to F_2. In contrast, when $h_d > \Delta h_0$, seepage occurred in the test soil layer, resulting in an increase in H_s above the bottom of the USM. Therefore, in the calculation of the buoyancy force from the groundwater in an aquitard, h_d minus Δh_0, should be used as H, while $\Delta h_0 = I_0 \times L_0$.

3.3. Validation of Δh_0

The scenario simulated in the MTB used in this study closely resembles that in the WBZ of a real-world aquitard in the city of Changchun. A test soil sample was taken from the construction site of the Underground Rail Transit Project of Changchun. The aquitard mainly consists of silty clay, for which the measured physical property metrics are presented in Table 3. To validate the hypothesis that $\Delta h_0 = I_0 \times L_0$, the variation in the H_s at different depths (equivalent to the H in a WBZ) and the stable H_0 in the MTB with h_d (equivalent to H_c) was monitored continuously along with F_2. First, the variation in H_s and Δh (i.e., h_d minus H_s) was analyzed to determine the values of Δh_0 at different depths, which were subsequently compared with the intercept of the fitting equation in Figure 9b. Then, the relationship between h_d and H_s was analyzed. Finally, the I_0 in the silty clay layer was determined through a laboratory test. On this basis, Δh_0 was calculated using Equation (5). Moreover, the measured and calculated values of Δh_0 were compared.

3.3.1. Variation in H_s and Δh

Figure 12 shows the variation in h_d and the H_s at each depth and their difference under instantaneous water-supply conditions. As seen in Figure 12, after h_d was increased instantaneously during each stage, the groundwater in the soil layer in the MTB began to seep. Consequently, H_s increased and eventually tended to stabilize. The variation in H_s was generally consistent with that in h_b. Moreover, after h_d was increased instantaneously during each stage, Δh peaked instantaneously and then gradually decreased until the seepage flow stopped. In this process, the Δh at each depth tended to be a nonzero stable value. Thus, as the groundwater transitioned from a seepage state to a static state, h_d remained higher than H_s. In addition, the Δh formed in a static state remained stable.

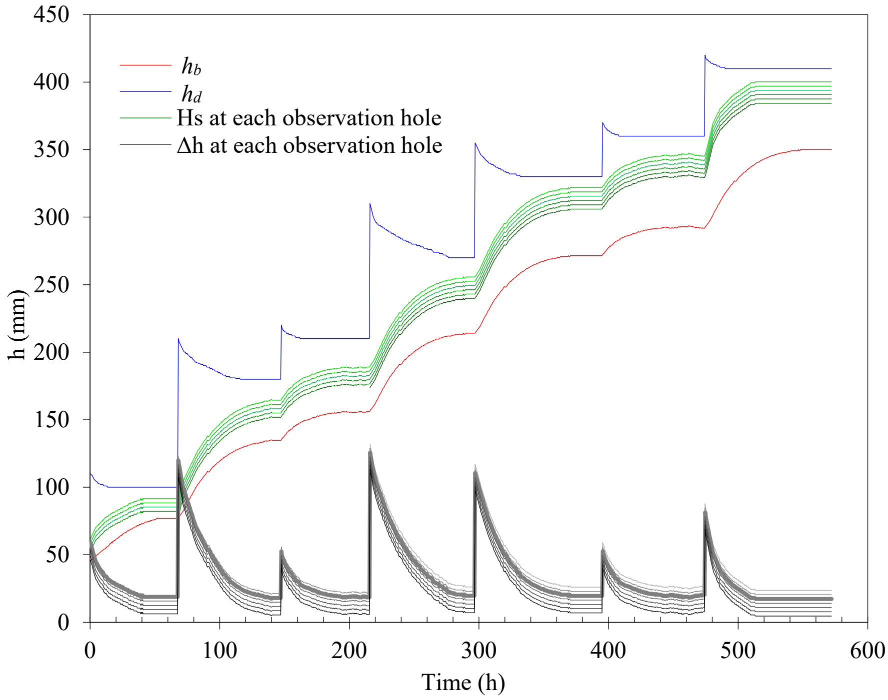

Figure 12. Curves showing the dynamic variation in H_s and Δh at different depths.

Table 4 summarizes the stable values of Δh at different depths at stages 1–7. At a depth of 400 mm, H_s observation hole G3 was located just below the bottom plate of the USM. The average value of Δh at observation hole G3 measured during the seven stages was 19.0 mm, which is almost identical to the intercept (19.2 mm) of the fitting equation in Figure 9b. This finding demonstrates that this transverse intercept is not a result of system error, but is instead the objectively existing Δh_0. Therefore, the stable Δh measured at the observation hole at each depth was the Δh_0 at this depth.

Table 4. Δh_0 and L_0 for observation holes at different depths and stages.

Observation Hole	Depth (mm)	L_0 (mm)	Δh_0 (mm)							
			Stage 1	Stage 2	Stage 3	Stage 4	Stage 5	Stage 6	Stage 7	Average
G1	200	800				27	26	27	25	26
G2	300	700		22	23	23	20	23	22	23
G3	400	600	18	19	20	19	18	20	19	19
G4	500	500	15	16	17	16	15	17	15	16
G5	600	400	12	13	12	13	13	14	13	13
G6	700	300	8	10	9	10	10	11	10	10
G7	800	200	6	5	6	7	7	7	5	6

Figure 13 shows the variation in Δh_0 at different depths during the multistage test process. Horizontally, the Δh_0 at any depth did not change appreciably as h_d increased. The corresponding broken line is almost a horizontal straight line. Vertically, Δh_0 and the corresponding L_0 both decreased as the depth increased. Therefore, Δh_0 is independent of h_d, but is closely linked with L_0.

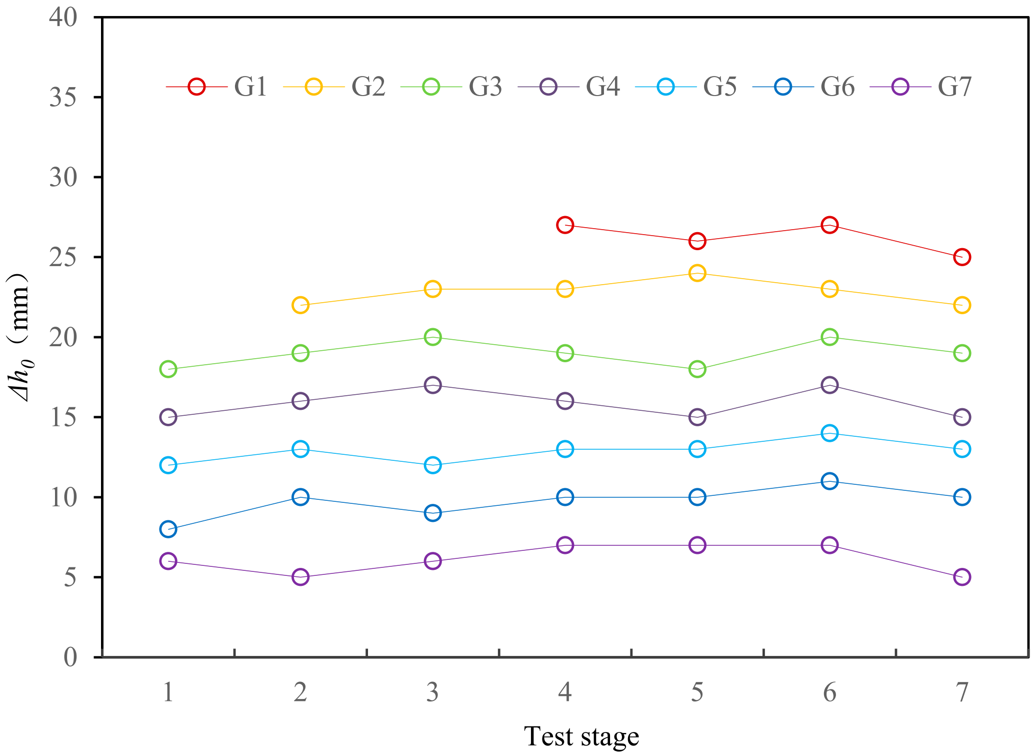

Figure 13. Variation in Δh_0 of the observation hole at different depths during the multistage test process.

3.3.2. Variation in the Stable h_d and H_0

After the groundwater entered a static state during each test stage, the stable H_0 was measured by drilling. The boreholes drilled at stages 1–7 are denoted by Z1–7. Figure 14 shows the stable h_d and H_0 at each stage. Analysis of Figure 14 shows the following. As the stable h_d increased, the stable H_0 and the thickness of the WBZ both increased. However, the stable H_0 was lower than the stable h_d at each stage. The Δh_0 in the WBZ of the test soil layer equaled the stable h_d minus the stable H_0. Table 5 summarizes the measured values of Δh_0 and the corresponding L_0. As seen in Table 5, an increase in L_0 led to an increase in Δh_0.

Table 5. Comparison of the stable h_d and H_0 in the MTB.

Test Stage	Borehole	Stable h_d (mm)	Stable H_0 (mm)	Δh_0 (mm)	L_0 (mm)
1	Z1	100	81	19	681
2	Z2	180	157	23	757
3	Z3	210	186	24	786
4	Z4	270	244	26	844
5	Z5	330	301	29	901
6	Z6	360	330	30	930
7	Z7	410	377	33	977

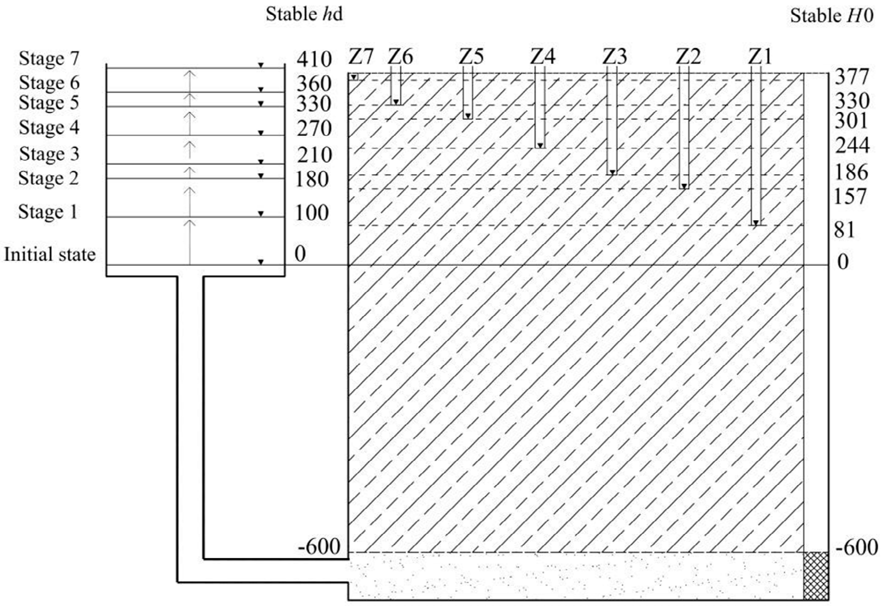

Figure 14. Schematic showing the stable h_d and H_0 (units: mm).

3.3.3. Comparison of the Theoretically Calculated and Measured Values of Δh_0

Six samples (denoted by 1–6) of the test silty clay layer used were analyzed in the laboratory to determine their I_0. Table 6 summarizes the test results. As shown in Table 6, the average I_0 in the test silty clay layer was 0.032. The theoretical value of Δh_0 corresponding to each value of L_0 in Tables 4 and 5 was calculated by multiplying the average I_0 by the value of L_0. Table 7 summarizes the calculation results. Figure 15 compares the theoretical and measured values of Δh_0. Analysis of Figure 15 reveals that the theoretical and measured values of Δh_0 basically fall near the 1:1 line and the correlation coefficient R_2 between them is 0.971, suggesting that the two values are nearly consistent. This finding demonstrates that $\Delta h_0 = I_0 \times L_0$.

Table 6. Test results for I_0 in the silty clay layer.

Test Sample	**1**	**2**	**3**	**4**	**5**	**6**	**Average**
I_0 (dimensionless)	0.031	0.033	0.035	0.033	0.029	0.032	0.032

Table 7. Theoretically calculated values of Δh_0 in the silty clay layer.

Observation Hole/Borehole	**Depth (mm)**	**L_0 (mm)**	**Theoretically Calculated Value of Δh_0 (mm)**
G1	200	800	26
G2	300	700	22
G3	400	600	19
G4	500	500	16
G5	600	400	13
G6	700	300	10
G7	800	200	6
Z1	319	681	22
Z2	243	757	24
Z3	214	786	25
Z4	156	844	27
Z5	99	901	29
Z6	70	930	30
Z7	23	977	31

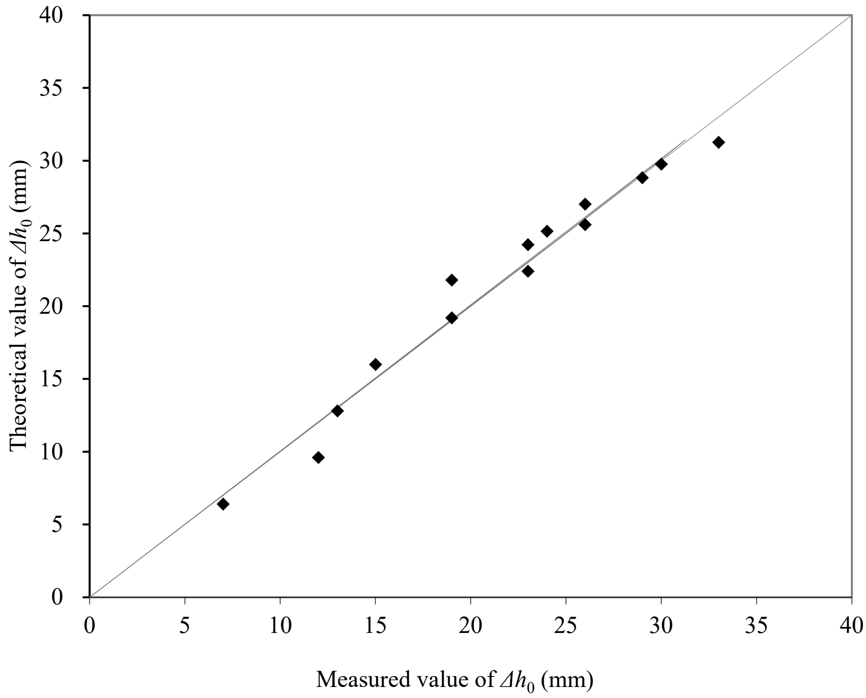

Figure 15. Comparison of the theoretically calculated and measured values ofΔh_0.

In summary, the above test results show that the groundwater level at any location in the WBZ of an aquitard is lower than the supply water level upstream of the seepage flow due to the action of I_0, that Δh_0 exists perennially, regardless of whether the groundwater is in a seepage or static state, and that $\Delta h_0 = I_0 \times L_0$. Therefore, the reduction in h due to Δh_0 should be considered in the calculation of the buoyancy force from the groundwater in an aquitard.

4. Conclusions

To address the difficulty in accurately estimating buoyancy resistance required for the construction of underground structures, model tests were conducted in this study to observe the buoyancy force on a USM in an aquitard. A phenomenon in geotechnical engineering, the occurrence of a Δh_0, was discovered and demonstrated based on observation data collected from real-world engineering settings and laboratory buoyancy tests. It was inferred from the laboratory buoyancy observation test data that a deviation from Darcy's law is the theoretical basis for Δh_0; that is, $\Delta h_0 = I_0 \times L_0$. A comparison shows a 1:1 linear correlation between the experimentally measured and theoretically calculated values of Δh_0, thus experimentally validating the theoretical explanation for Δh_0. The results of this study provide a basis for scientifically calculating the buoyancy resistance required for the construction of underground structures.

Author Contributions: Conceptualization, C.D. and Y.X.; methodology, Y.X.; validation, W.P. and S.H.; formal analysis, Y.X. and S.L.; investigation, C.D.; resources, H.M. and Y.X.; data curation, H.M.; writing—original draft preparation, Y.X.; writing—review and editing, C.D.; visualization, S.H. and S.L.; supervision, C.D. All authors have read and agreed to the published version of the manuscript.

Funding: This research was funded by the Open Research Fund Program the Beijing Key Laboratory of Geotechnical Engineering for Deep Foundation Pit of Urban Rail Transit (202103).

Institutional Review Board Statement: This study does not require ethical approval.

Informed Consent Statement: Not applicable.

Data Availability Statement: The data presented in this study are available in this article.

Acknowledgments: The authors would like to thank Jianquan Zhang and Wenxin Gao for the suggestions and support in this research.

Conflicts of Interest: The authors declare no conflict of interest.

Abbreviations

PWP	Pore-water pressure
USM	Underground structure module
MTB	Model test box
ESM	Enclosure structure module
Symbols	
Δh	Hydraulic head difference
Δh_0	Initial hydraulic head difference
I	Hydraulic gradient
I_0	Initial I
L_0	Length of the corresponding seepage path
H_s	Head of the test soil layer
H_0	Stable initial head
H_c	Confined head in the aquifer
G_0	Dead weight of the USM
F_1	Vertical reaction of soil particles
F_2	Buoyancy force exerted by groundwater
P_s	Pressure detected by the tension–compression sensor
P_{s0}	The force on the soil sample the when the buoyancy from the groundwater is zero
A	Area of the bottom of a rigid circular steel plate
G	Gravitational acceleration
h_b	Buoyancy head from groundwater
h_d	Delivery head

References

1. Bikçe, M.; Örnek, M.; Cansız, Ö.F. The effect of buoyancy force on structural damage: A case study. *Eng. Fail. Anal.* **2018**, *92*, 553–565. [CrossRef]
2. Tang, H.Y.; Yang, D.; Wang, C.J.; Guo, H.X.; Dong, Q.P. Anti-floating problem and retrofit measures for a damaged basement. *Mater. Res. Innov.* **2015**, *19*, S8-219–S8-222. [CrossRef]
3. Zhou, J.K.; Lin, C.H.; Chen, C.; Zhao, X.Y. Reduction of groundwater buoyancy on the basement in weak-permeable/impervious foundations. *Adv. Civil. Eng.* **2019**, *2019*, 7826513. [CrossRef]
4. Huerta, D.A.; Sosa, V.; Vargas, M.C.; Ruiz-Suárez, J.C. Archimedes' principle in fluidized granular systems. *Phys. Rev. E* **2005**, *72*, 031307. [CrossRef] [PubMed]
5. dos Santos, F.C.; Santos, W.M.S.; Berbat, S.D. An analysis of floating bodies and the principle of archimedes. *Rev. Bras. Ensino Fis.* **2007**, *29*, 295–298.
6. Barbot, A.; Lopes, J.B.; Soares, A.A. Relating water and energy by experimenting with urban water cycle, desalination of sea water and archimedes' law. In Proceedings of the 6th International Technology, Education and Development Conference, Valencia, Spain, 5–7 March 2012; pp. 2534–2544.
7. Kang, W.T.; Feng, Y.J.; Liu, C.S.; Blumenfeld, R. Archimedes' law explains penetration of solids into granular media. *Nat. Commun.* **2018**, *9*, 1101. [CrossRef]
8. Hisatake, M. A Proposed methodology for analysis of ground settlements caused by tunneling, with particular reference to the "buoyancy" effect. *Tunn. Undergr. Space Technol.* **2011**, *26*, 130–138. [CrossRef]
9. Liu, X.Y.; Yuan, D.J. Mechanical analysis of anti-buoyancy safety for a shield tunnel under water in sands. *Tunn. Undergr. Space Technol.* **2015**, *47*, 153–161. [CrossRef]
10. Xu, Z.J.; Yu, H.H. Non-contact experiment investigation of the interaction between the soil and underground granary subjected to water buoyancy. *Appl. Sci.* **2021**, *11*, 8988. [CrossRef]
11. Zhang, J.W.; Cao, J.; Mu, L.; Wang, L.; Li, J. Buoyancy force acting on underground structures considering seepage of confined water. *Complexity* **2019**, *2019*, 7672930. [CrossRef]
12. Zhang, D.; Chen, L. Experiment on the computing method of anti-floating in underground structures. *Sichuan Build. Sci.* **2008**, *34*, 105–108. (In Chinese)
13. Li, X.L.; Wang, B.L.; Li, X.; Ji, C. Analysis of anti-floating measures and construction parameters of shield tunnel through river under ultra-shallow covering. In Proceedings of the International Conference on Civil Engineering, Architecture and Building Materials, Jinan, China, 24–26 May 2013; pp. 628–634.

14. Zhang, S.Q.; Yuan, W.J.; Zhang, H.H.; Huang, L.; Zhong, Y.F. Analytical and numerical anti-floating study concerning the shield tunnel across the river. In Proceedings of the International Conference on Structures and Building Materials, Guiyang, China, 9–10 March 2013; pp. 1087–1092.
15. Tang, M.X.; Hu, H.S.; Zhang, C.L.; Hou, M.X.; Chen, H. Determination of anti-floating water level in guangzhou based on the distribution of the underground aquifers. In Proceedings of the GeoShanghai International Conference on Geoenvironment and Geohazard, Shanghai, China, 27–30 May 2018; pp. 468–480.
16. Cui, Y.; Cui, J.; Wu, S. A model test of shallow underground structure buoyancy. *Spec. Struct.* **1999**, *16*, 32–36. (In Chinese)
17. Xiang, K.; Zhou, S.; Zhan, C. Model test study of buoyance on shallow underground structure. *J. Tongji Univ. (Nat. Sci.)* **2010**, *38*, 346–352. (In Chinese)
18. Zhou, P. Groundwater Uplift Mechanism Study under Complex Urban Environment. Master's Thesis, China University of Geosciences (Beijing), Beijing, China, 2006.
19. Song, L.; Kang, X.; Mei, G. Buoyancy force on shallow foundations in clayey soil: An experimental investigation based on the "Half Interval Search". *Ocean. Eng.* **2017**, *129*, 637–641. [CrossRef]
20. Song, L.; Huang, Q.; Yan, D.; Mei, G. Experimental study on effect of hydraulic gradient on permeability of clay. *Chin. J. Geotech. Eng.* **2018**, *40*, 1635–1641. (In Chinese)
21. Zhang, Q.; Ouyang, L.; Wang, Z.; Liu, H.; Zhang, Y. Buoyancy reduction coefficients for underground silos in sand and clay. *Indian Geotech. J.* **2019**, *49*, 216–223. [CrossRef]
22. Zhang, Z.; Cao, P.; Jia, M. Centrifugal model test of pore water pressure in soft clay. In Proceedings of the GeoShanghai 2018 International Conference: Fundamentals of Soil Behaviours, Shanghai, China, 28–30 May 2018.
23. Zhang, Z. *The Bond Water Dynamics Theory*; Geology Press: Beijing, China, 1980; pp. 80–83.
24. Kutílek, M. Non-darcian flow of water in soils—Laminar region: A review. *Dev. Soil Sci.* **1972**, *2*, 327–340.
25. Mesri, G.; Rokhsar, A. Theory of consolidation for clays. *J. Geotech. Geoenviron. Eng.* **1974**, *100*, 889–904.
26. Deng, Y.; Xie, H.; Huang, R.; Liu, C. Law of nonlinear flow in saturated clays and radial consolidation. *Appl. Math. Mech.* **2007**, *28*, 1427–1436. [CrossRef]
27. Law, K.T.; Lee, C.F. Initial gradient in a dense glacial till. In Proceedings of the 10th International Conference on Soil Mechanics and Foundation Engineering, Stockholm, Sweden, 15–19 June 1981; Volume 1, pp. 441–446.